

Hybrid Quantum-inspired Resnet and Densenet for Pattern Recognition

Andi Chen^{a,b}, Hua-Lei Yin^{c,*}, Zeng-Bing Chen^{b,*}, Shengjun Wu^{a,b,*}

^a*Institute for Brain Sciences and Kuang Yaming Honors School, Nanjing University, Nanjing 210023, China*

^b*National Laboratory of Solid State Microstructures and School of Physics, Collaborative Innovation Center of Advanced Microstructures, Nanjing University, Nanjing 210093, China*

^c*School of Physics and Beijing Key Laboratory of Opto-Electronic Functional Materials and Micro-Nano Devices, Key Laboratory of Quantum State Construction and Manipulation(Ministry of Education), Renmin University of China, Beijing 100872, China*

Abstract

In this paper, we propose two hybrid quantum-inspired neural networks with adaptive residual and dense connections respectively for pattern recognition. We explain the frameworks of the symmetrical circuit models in the quantum-inspired layers in our hybrid models. We also illustrate the potential superiority of our hybrid models to prevent gradient explosion owing to the quantum-inspired layers. Groups of numerical experiments on generalization power show that our hybrid models possess roughly the same level of generalization power as the pure classical models with different noisy datasets utilized. Furthermore, the comparison on generalization ability between our hybrid models and a state-of-the-art hybrid quantum-classical convolutional network demonstrates 3%-4% higher accuracy of our hybrid densely-connected model than the hybrid quantum-classical network. Simultaneously, in terms of groups of experiment on robustness, the results demonstrate that our two hybrid models outperform pure classical models notably in resistance to parameter attacks with various asymmetric noises. They also indicate the superiority of our densely-connected hybrid model over the hybrid quantum-classical network under both symmetrical and asymmetrical attacks. Furthermore, an ablation study indicate that the recognition accuracy of our two hybrid models is 2%-3% higher than that of the traditional quantum-inspired neural network without residual or dense connection. Eventually, we discuss the application scenarios of our hybrid models by analyzing their computational complexities.

Keywords: hybrid neural network, residual and dense connections, pattern recognition, gradient explosion, generalization power, robustness

1. Introduction

As the cornerstone of AI technology, deep neural network algorithms have played a pivotal role over the past few decades [1, 2, 3, 4, 5, 6, 7]. Typical models incorporate deep residual and dense networks (Resnet and Densenet) in image recognition, Large Language Models (LLM) in natural language processing, and Sora model

in multi-modal generations [8, 9, 10, 11]. Nevertheless, due to the limited generalization power and robustness of classical neural networks, the design of neural networks with stronger generalization power and robustness over pure classical models is tremendously expected nowadays [12, 13, 14, 15, 16]. Simultaneously, quantum-inspired neural networks, which obey the laws of quantum computing and deep learning, appear with their prominent performances on certain circumstances [17, 18, 19]. Innovative frameworks include quantum-inspired stochastic walks and variational circuit models, etc [19, 20, 21, 22].

*corresponding author

Email addresses: andynju1999@gmail.com (Andi Chen^{a,b}), hlyin@ruc.edu.cn (Hua-Lei Yin^{c,*}), zbchen@nju.edu.cn (Zeng-Bing Chen^{b,*}), sjwu@nju.edu.cn (Shengjun Wu^{a,b,*})

What's more, to improve the universality of the quantum-inspired models under complex environments, hybrid quantum-inspired neural networks have been explored in some studies [23, 24, 25, 26]. Connected with classical convolutional layers, they demonstrate remarkable performance on image detection and other tasks[27, 28, 29]. Comprised of the pure classical part and the quantum-inspired part, they could leverage different advantages from both pure classical and quantum-inspired neural networks [25, 26].

Nevertheless, despite a few works of hybrid quantum-inspired neural networks, there is a lack of them which leverage the amalgamation of circuit models and residual or dense connection [8, 9, 30]. Hence, we firstly design the hybrid **Quantum-inspired Residual Feedforward Neural Network** (QRFNN) and hybrid **Quantum-inspired Dense Feedforward Neural Network** (QDFNN). We also devise hybrid **Quantum-inspired Residual Convolutional Neural Networks** (QRCNN) and hybrid **Quantum-inspired Dense Convolutional Neural Networks** (QDCNN) for image problems. We apply our four hybrid models on pattern classification problems. A **Hybrid Quantum-classical convolutional Network** (HQNet), classical **Multi-Layer Perceptrons** (MLPs) and **Convolutional Neural Networks** (CNNs) with detailed structures serve as state-of-the-arts for model comparison. Hence, in the paper, we:

- design and analyze QRFNN and QDFNN for recognition of iris data [31] under noisy and noiseless environments;
- design and analyze QRCNN and QDCNN for classification of MNIST, FASHIONMNIST and CIFAR image datasets [31] under noisy and noiseless environments;
- conduct assorted numerical experiments to compare our hybrid models with a state-of-the-art hybrid quantum-classical convolutional network and pure

classical models;

- implement an ablation study to compare our hybrid models with traditional quantum-inspired neural networks without residual or dense connection on pattern recognition;
- discuss the advantages and illustrate the application scenarios of our hybrid models owing to their frameworks and their computational complexities.

Next, in section 2, we review the corresponding works of classical residual and dense frameworks and quantum-inspired neural networks with circuit models. In section 3, we introduce some basic concepts of circuit models, residual structure and dense structure [8, 9, 30]. As for section 4, we explain our hybrid models including the layer details and parameter learning details. Following it, some numerical experiments are implemented in section 5, which involve comparisons between our hybrid models and pure classical and the hybrid quantum-classical models. We also do an ablation study incorporating comparisons between our hybrid models and the quantum-inspired neural network without residual or dense connection in section 5. Finally, we illustrate the application scenarios and some future work of our hybrid models in section 6.

2. Related Work

2.1. Residual and dense frameworks

The original deep neural network for pattern recognition, Alexnet, was proposed in 2012 [32]. In spite of the outstanding performance of deep networks in complicated problems [33, 34, 35, 36, 37, 38, 39, 40], experimental findings had also underscored the trouble in training deep neural networks without residual or dense connection, such as feature disappearance [1, 2, 8, 9]. Consequently, Resnet and Densenet, which were firstly introduced in 2016, showed outstanding performance in image classification [8, 9]. The residual and dense frameworks imply the superiority of the element-wise addition mechanism

and the feature map concatenation mechanism separately. Additionally, both of the two approaches show a great capacity to mitigate feature vanishing and overcome gradient vanishing [2, 8, 9]. Large-scale models such as YOLO in autonomous driving and attention-based Transformer in text translation, draw inspiration from these seminal works [34, 41]. Therefore, the residual and dense connections may facilitate feature propagation and enhance the universality of the quantum-inspired part of our hybrid models as well. Nevertheless, if there is some noise in the datasets, the original residual and dense frameworks may also possess the potential to transmit the noise information to the output layer while transferring the feature of the data itself, thereby interfering with recognition accuracy [1]. Therefore, different from the original residual and dense architectures, we propose two adaptive residual and dense connections with adaptive parameters λ that can update themselves by back propagation to reduce the impacts of noise. And we embed the adaptive residual and dense architectures into the quantum-inspired layers of our hybrid models.

2.2. Quantum-inspired neural networks with circuit models

Quantum-inspired neural networks, a classical algorithm essentially, are impacted by some quantum laws [21, 22]. A typical model is circuit model [22, 42]. In the authentic quantum circuit system, classical data is encoded into a quantum state. And the data feature is acquired via evolutionary processes and stored in the parameters in the unitary gates of the circuit models. And the design of the quantum-inspired part of our hybrid models draw on the frameworks of the circuit models in authentic quantum system [22]. Moreover, our quantum-inspired layers only follows some laws of circuit models, therefore, our hybrid models require more improvements to be deployed on authentic quantum computers. However, in previous studies of circuit models, the architectures of the circuits are

usually unsymmetrical, which may result in information loss [22]. Moreover, the unitary gates utilized incorporate R_Y , R_Z , Hadamard and CNOT gates, some of which contain no parameter and could not assist feature learning [25, 26, 42]. Hence, to enable our models to fully extract the feature, each gate in the quantum-inspired part contains a parameter. Moreover, one novelty lies in the proposal of the symmetrical "V" shape in each quantum-inspired layer of our hybrid models in Fig.3, which may also help feature storage [19, 43]. In addition, traditional quantum-inspired networks may not possess very outstanding learning capability [21], thus another novelty lies in the combination of the adaptive residual and dense connections and the symmetrical circuit models.

3. Preliminary

3.1. Circuit models

Analogous to classical bit in classical computers, a qubit, the unit in quantum-inspired algorithms, is described as a 2-dimensional complex vector in Hilbert space [22]. It can be described according to the superposition rules:

$$|\psi\rangle = a|0\rangle + b|1\rangle, \quad |a|^2 + |b|^2 = 1 \quad (a, b \in \mathbb{C}). \quad (1)$$

In our hybrid frameworks, the evolution process stands for the manipulation to the quantum states with continuous unitary operations:

$$|\psi_m\rangle = U_m |\psi_{m-1}\rangle \quad (m \in \mathbb{N}^+), \quad (2)$$

where U_m represents the $(m+1)^{th}$ unitary gate in the m^{th} evolution. And $|\psi_0\rangle$ means the initial state. The gate

utilized in the paper, $T_i(\theta_r^{l-1})$:

$$= i \begin{pmatrix} 1 & 0 & \cdots & \cdots & \cdots & \cdots & 0 \\ 0 & 1 & & & & & \vdots \\ \vdots & & \ddots & & & & \vdots \\ & & & \cos(\theta_r^{l-1}) & -\sin(\theta_r^{l-1}) & & \vdots \\ & & & \sin(\theta_r^{l-1}) & \cos(\theta_r^{l-1}) & & \vdots \\ \vdots & & & & & \ddots & \vdots \\ 0 & \cdots & \cdots & \cdots & \cdots & \cdots & 1 & 0 \\ & & & & & & 0 & 1 \end{pmatrix} \quad (3)$$

As for Eq.(3), i denotes the row index of the term $-\sin(\theta_r^{l-1})$, also the column index of the term $\sin(\theta_r^{l-1})$ ($i \in \mathbb{N}^+$). And θ_r^{l-1} means the $(r+1)^{th}$ parameter in the l^{th} layer ($r \in \mathbb{N}, l \in \mathbb{N}^+$). And r has relations with i , which is shown in Eq.(4).

3.2. Resnet and Densenet learning

Realizing the possible impacts from the noise, we propose linear addition mechanism with adaptive parameters [2, 8]. In terms of the residual framework, Fig.1 shows its partial structure. $H_h(x) = R_{h-1}(H_{h-1}(x)) \oplus \lambda_{h-1}H_{h-1}(x)$ ($h \in \mathbb{N}^+$), where \oplus means linear element-wise addition, R_{h-1} is the residual mapping of the h^{th} layer. And λ_{h-1} is the adaptive parameter of H_{h-1} in the h^{th} layer. And the dense framework in this paper also emanates from the element-wise addition mechanism of all the preceding layers in Fig.2, where $G_a(x) = D_{a-1}(G_{a-1}(x)) \oplus \lambda_{a,0}x \oplus \sum_{b=1}^{a-1} \lambda_{a,b}G_b(x)$ ($a, b \in \mathbb{N}^+$) for more layers. D_{a-1} refers to dense mappings of the a^{th} layer. $\lambda_{a,0}$ and $\lambda_{a,b}$ are the adaptive parameters of x and $G_b(x)$ respectively.

4. Hybrid Quantum-inspired Resnet and Densenet

We describe our hybrid models with specific architectures in this section, which include layer details of QRFNN and QDFNN and parameter learning of QRFNN and QDFNN.

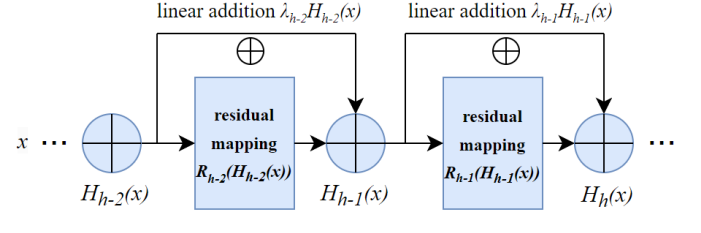


Figure 1: Adaptive residual connection

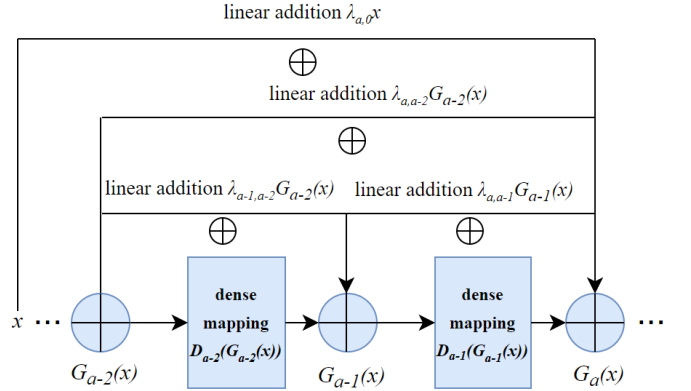


Figure 2: Adaptive dense connection

4.1. Layer details of QRFNN and QDFNN

Fig.3 demonstrates the QRFNN and QDFNN structures of 2 qubits with 2 layers, where each line represents one-dimensional vector space of a quantum state. The green, blue circles denote the input and output neurons respectively. To consider the general occasions, suppose we build L quantum-inspired layers, the quantum-inspired part, as hidden layers, in QRFNN and QDFNN rather than MLP hidden layers with neurons. So there are $L+2$ layers totally in both QRFNN and QDFNN. We set the quantum states in the quantum-inspired layers are N -dimensional with n qubits utilized for QRFNN and QDFNN ($2^{n-1} \leq N \leq 2^n$). And $T_i(\theta_r^l) \in \mathbb{R}^{N \times N}$. We also suppose the dimension of the input, $X = (x_0, x_1, \dots, x_{N-1})^\top$, is N . In terms of r and i in Eq.(3) in this section, we also have:

$$r = \begin{cases} i-1 & 0 \leq r \leq N-2 \\ 2N-3-i & N-2 < r \leq 2N-4 \end{cases} \quad (4)$$

Therefore, the row and parameter indices in Eq.(3) can be represented with only one variable simultaneously. For

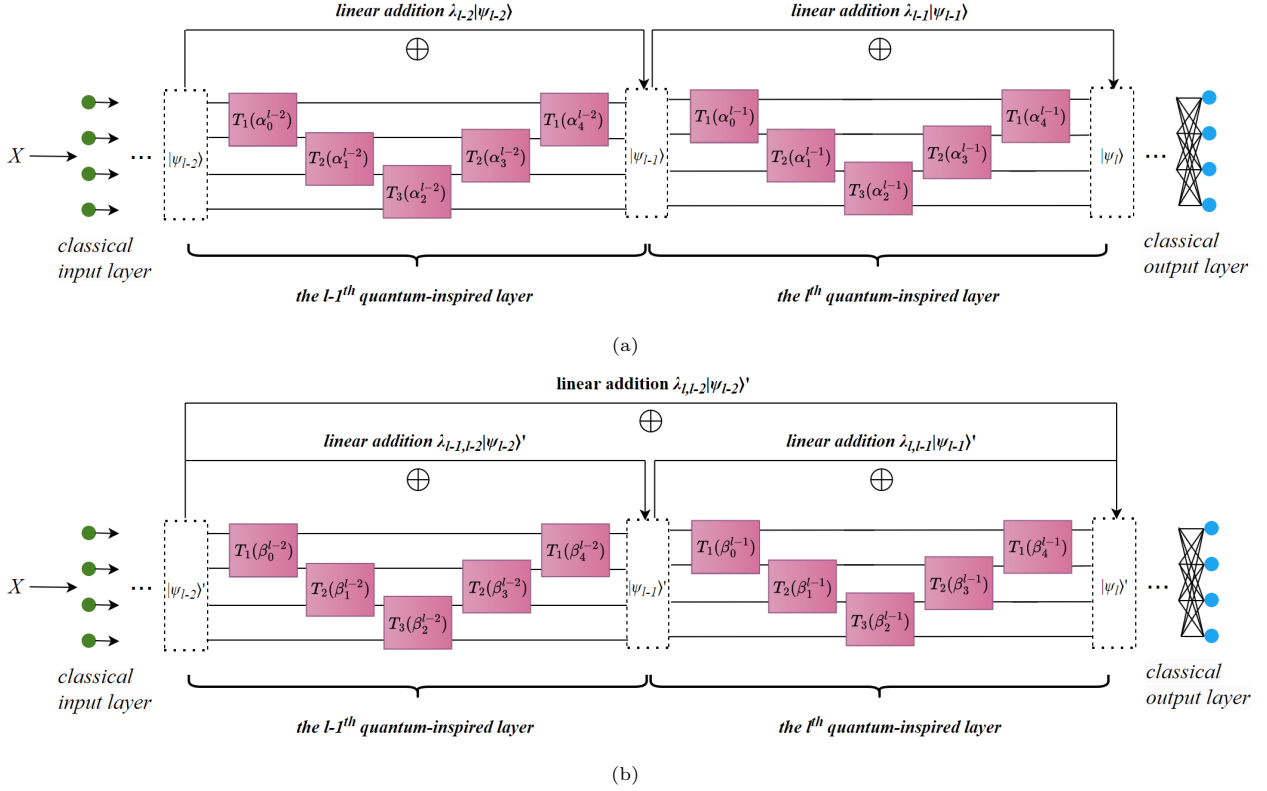


Figure 3: QRFNN and QDFNN. (a) QRFNN. (b) QDFNN.

multiplication of the T matrices in the l^{th} quantum-inspired layer, we define:

$$\prod_{j=0}^{j=N} T_{j+1}(\alpha_j^{l-1}) := T_1(\alpha_0^{l-1})T_2(\alpha_1^{l-1})\dots T_{N+1}(\alpha_N^{l-1}) \quad (5a)$$

$$\prod_{j=0}^{j=N} T_{j+1}(\beta_j^{l-1}) := T_1(\beta_0^{l-1})T_2(\beta_1^{l-1})\dots T_{N+1}(\beta_N^{l-1}) \quad (5b)$$

For the l^{th} quantum-inspired layer, we define:

$$U_{l-1} := \left(\prod_{j=0}^{j=N-2} T_{j+1}(\alpha_j^{l-1}) \right) \times \left(\prod_{j=N-1}^{j=2N-4} T_{2N-3-j}(\alpha_j^{l-1}) \right), \quad (6a)$$

$$U'_{l-1} := \left(\prod_{j=0}^{j=N-2} T_{j+1}(\beta_j^{l-1}) \right) \times \left(\prod_{j=N-1}^{j=2N-4} T_{2N-3-j}(\beta_j^{l-1}) \right), \quad (6b)$$

where α_j^{l-1} and β_j^{l-1} are the $(j+1)^{th}$ parameters in the l^{th} layer of QRFNN and QDFNN separately. And U_{l-1} , U'_{l-1} are the multiplications of all the unitary gates in the l^{th} quantum-inspired layer of QRFNN and QDFNN separately. And the general framework of the l^{th} quantum-

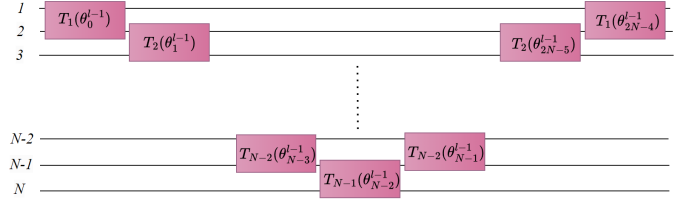


Figure 4: General structure of the l^{th} quantum-inspired layer. Here the parameter is represented as θ , but in QRFNN and QDFNN, we use α and β as parameters respectively. And each line represents one-dimensional vector space of the states. Furthermore, the "V" shape helps feature learning of each category of the dataset. On one hand, if the circuit shape is not the symmetrical "V" shape, there could be imbalance of the number of parameters of each category of a dataset for feature learning. On the other hand, each unitary gate is a sparse matrix with only one parameter, which ensure the convenience of computation and guarantee that over-parameterization does not occur.

inspired layer is shown as Fig.4.

As for the evolution process, firstly, X is input into the neurons of the input layer, then we encode the information of X into the amplitude of $|\psi_0\rangle$ of QRFNN and $|\psi_0\rangle'$ of

QDFNN:

$$\eta = \sqrt{\sum_{k=0}^{N-1} x_k^2}, \quad (7a)$$

$$|\psi_0\rangle = \sum_{k=0}^{N-1} \frac{x_k}{\eta} |k\rangle, \quad (7b)$$

$$|\psi_0\rangle' = \sum_{k=0}^{N-1} \frac{x_k}{\eta} |k'\rangle, \quad (7c)$$

where we represent $|k\rangle$ and $|k'\rangle$ using the binary representation $k = k_{n-1}k_{n-2}\dots k_0$. More formally, $k = \sum_{j=0}^{n-1} k_j 2^j$. Secondly, as shown in Fig.3, in terms of QRFNN:

$$|\psi_l\rangle = U_{l-1} |\psi_{l-1}\rangle \oplus \lambda_{l-1} |\psi_{l-1}\rangle \quad (1 \leq l \leq L). \quad (8)$$

While for QDFNN:

$$|\psi_l\rangle' = U'_{l-1} |\psi_{l-1}\rangle' \oplus \sum_{j=0}^{j=l-1} (\lambda_{l,j} |\psi_j\rangle') \quad (1 \leq l \leq L), \quad (9)$$

and $|\psi_l\rangle, |\psi_l\rangle'$ are respectively the output states of the l^{th} quantum-inspired layers of QRFNN and QDFNN. \oplus denotes the element-wise addition mechanism. The terms $U_{l-1} |\psi_{l-1}\rangle$ and $U'_{l-1} |\psi_{l-1}\rangle'$ indicate the quantum-inspired parts of the two models obey laws of circuit models [22]. However, because our hybrid models also follow the deep learning laws, $|\psi_l\rangle$ and $|\psi_l\rangle'$ can be also respectively represented as column vectors O_l and O'_l (see supplementary materials part 2). For QRFNN, $O_l = (o_{l,0}, o_{l,1}, \dots, o_{l,N-1})^\top$. For QDFNN, $O'_l = (o'_{l,0}, o'_{l,1}, \dots, o'_{l,N-1})^\top$. And $o_{l,j}, o'_{l,j}$ denote the output at the $(j+1)^{th}$ dimensional index of the l^{th} quantum-inspired hidden layer of the two models respectively. And we have:

$$o_{l,j} = \sum_{j=0}^{N-1} (v_j \cdot o_{l-1,j}), \quad (10a)$$

$$o'_{l,j} = \sum_{j=0}^{N-1} (v'_j \cdot o'_{l-1,j}), \quad (10b)$$

where v_j , the coefficient of $o_{l-1,j}$, is the linear summations of many terms, where each term is the multiplication of $\lambda_{l-1}, \sin(\alpha_r^{l-1}), \cos(\alpha_r^{l-1})$ and the input data. Similarly, v'_j , the coefficient of $o'_{l-1,j}$, is also the linear summations

of many terms, where each term is the multiplication of $\lambda_{l,l-1}, \sin(\beta_r^{l-1}), \cos(\beta_r^{l-1})$ and the input data. The output of the last quantum-inspired layer of QRFNN and QDFNN is O_L and O'_L respectively. Eventually, the final outputs will be:

$$O_{L+1} = \sigma((W_{L+1} \cdot O_L)^\top + B_{L+1}), \quad (11a)$$

$$O'_{L+1} = \sigma((W'_{L+1} \cdot O'_L)^\top + B'_{L+1}), \quad (11b)$$

where σ denotes any activation function, W_{L+1} and W'_{L+1} mean the weight matrices of the output layers of QRFNN and QDFNN separately, while B_{L+1}, B'_{L+1} represent biases of QRFNN and QDFNN respectively. Therefore, our hybrid neural networks are comprised of quantum-inspired hidden layers, as well as pure classical input and output layers.

4.2. Parameter learning of QRFNN and QDFNN

In the part 1 of the supplementary material, the framework of the MLP is also given. By comparison, it is found that the similarity of QRFNN, QDFNN and MLP lies in the feedforward layer-by-layer transfer of features. What's more, the classical output layer with activation functions and biases further enhances the ability of our hybrid models for nonlinear problems [2]. It also makes sense to activate the quantum-inspired layers with varied activation functions. The advantage of the classical input and output layers of QRFNN and QDFNN is the convenience of changing the number of neurons. Hence, our hybrid models are capable of allowing inputs and outputs of different dimensions. In addition, on the basis of the chain rule [2], the gradients of loss functions to the parameter α_r^{l-1} and β_r^{l-1} are given:

$$\frac{\partial(\text{loss})}{\partial \alpha_r^{l-1}} = \frac{\partial(\text{loss})}{\partial O_{L+1}} \cdot \left(\prod_{j=0}^{L-l} \frac{\partial O_{L+1-j}}{\partial O_{L-j}} \right) \cdot \frac{\partial O_l}{\partial \alpha_r^{l-1}}, \quad (12a)$$

$$\frac{\partial(\text{loss}')}{\partial \beta_r^{l-1}} = \frac{\partial(\text{loss}')}{\partial O'_{L+1}} \cdot \left(\prod_{j=0}^{L-l} \frac{\partial O'_{L+1-j}}{\partial O'_{L-j}} \right) \cdot \frac{\partial O'_l}{\partial \beta_r^{l-1}}, \quad (12b)$$

where loss and loss' denote the loss functions of QRFNN and QDFNN separately. The terms, $\frac{\partial O_{L+1-j}}{\partial O_{L-j}}$ and $\frac{\partial O'_{L+1-j}}{\partial O'_{L-j}}$

$(0 \leq j \leq L-l)$, are derivative matrices. And each element in each of the matrices involves additions and multiplications of many sine and cosine functions. Because the ranges of sine and cosine functions are both [-1,1], there are limitations of the absolute value of each element in each of the matrices, which makes the absolute value of each element not very large. As a result, the absolute values of $\frac{\partial(\text{loss})}{\partial \alpha_r^{l-1}}$ and $\frac{\partial(\text{loss})}{\partial \beta_r^{l-1}}$ will be not very large, either. On the other hand, a common problem at deep learning region, gradient explosion, is caused by very large values of the gradients of the loss functions to the parameters [2]. As a result, the parameters in the neural networks are unable to be updated and the neural networks are not capable of learning features of new data. However, our hybrid models may be able to prevent gradient explosion through this theoretical analysis. More details of the illustration of our hybrid models to prevent gradient explosion are in the part 4 of the supplementary material.

5. Numerical experiments

In this section, we validate the generalization power of our hybrid models with various datasets. We also illustrate the robustness of our hybrid models with various parameter attacks utilizing noise. The programming architecture we use is Pytorch. Two MLPs with different activation functions are used for comparison with QRFNN and QDFNN. The details of the MLPs are in part 1 and 10 of the supplementary material. HQNet and Two CNNs with different activation functions are used for comparison with QRCNN and QDCNN in generalization power and robustness test. In terms of HQNet proposed in 2024, it indicated higher accuracy and f1 score over AG-CNN and other advanced convolutional networks on large MRI image classification tasks [2, 27]. Its hybrid framework is similar with our QRCNN and QDCNN. Hence, we consider HQNet as the state-of-the-art hybrid models for comparison. Besides that, we also reduce the size of the original HQNet utilizing 2 qubits to apply to smaller-size image

classification. SPDA module of the convolutional part are utilized in the original HQNet. Additionally, we use parallel spatial and channel attention with residual or dense connection in the convolutional part in our HQNet, which is exactly the same as that in QRCNN (see part 6 of the supplementary material for more details of the convolutional part). And we maintain the architectures of the random circuit of the feedforward part in our HQNet due to the distinguished performance of it [27]. We use R_x and CR_x gate to construct the random circuit in HQNet (see part 13 of the supplementary material) [27]. When it comes to the two classical CNNs, they are constituted by convolutional layers and fully connected layers with MLPs. And QRCNN is comprised of residually-connected convolutional layers and fully connected layers with QRFNN, and QDCNN is comprised of densely-connected convolutional layers and fully connected layers with QDFNN. The convolutional parts in CNNs and QRCNN are identical. And we set most of the hyperparameters including learning rate, the number of fully connected layers of our HQNet, CNNs, QDCNN and QRCNN the same to compare these models more accurately (see part 10 of the supplementary material). Moreover, an ablation study is also conducted to test the superiority of the residual and dense connections. The traditional quantum-inspired neural network without residual or dense connection is utilized for comparison in it. All the results in this chapter are testing results.

5.1. Generalization power test

Generalization power is appraised by accuracy, precision, recall, f1 score, P-R curve area and ROC curve area [2]. Precision refers to the proportion of samples that are actually positive among all samples predicted to be positive by the model, while recall represents the proportion of samples that the model can correctly predict to be positive among all samples that are actually positive [1]. And f1 score is an important indicator for balancing recall and

Table 1: Results on FASHIONMNIST with gaussian symmetrical noise

	QRCNN	CNN(leaky-relu)	QDCNN	CNN(rot-relu)
P-R curve area	0.9730	0.9766	0.9768	0.9788
ROC curve area	0.9892	0.9911	0.9910	0.9917
Accuracy	0.9284±0.0179	0.9299±0.0177	0.9316±0.0175	0.9310±0.0176

Table 2: Results of category 0 of FASHIONMNIST with gaussian symmetrical noise

		QRCNN	CNN(leaky-relu)	QDCNN	CNN(rot-relu)
variance	recall	1.290E-02	1.163E-02	9.408E-03	1.437E-02
	precision	1.110E-02	1.062E-02	1.001E-02	1.008E-02
	f1 score	6.558E-03	6.547E-03	5.022E-03	7.114E-03
mean value	recall	0.9220	0.9206	0.9331	0.9144
	precision	0.8982	0.9102	0.9076	0.9108
	f1 score	0.9018	0.9091	0.9136	0.9049

Table 3: Results of category 1 of FASHIONMNIST with gaussian symmetrical noise

		QRCNN	CNN(leaky-relu)	QDCNN	CNN(rot-relu)
variance	recall	4.551E-03	6.904E-03	3.570E-03	5.179E-03
	precision	3.872E-03	3.742E-03	3.936E-03	3.862E-03
	f1 score	2.385E-03	3.470E-03	2.070E-03	3.168E-03
mean value	recall	0.9751	0.9702	0.9801	0.9805
	precision	0.9642	0.9647	0.9655	0.9657
	f1 score	0.9672	0.9638	0.9705	0.9703

Table 4: Results of category 2 of FASHIONMNIST with gaussian symmetrical noise

		QRCNN	CNN(leaky-relu)	QDCNN	CNN(rot-relu)
variance	recall	1.210E-02	1.408E-02	9.901E-03	1.254E-02
	precision	5.680E-03	6.067E-03	5.179E-03	7.347E-03
	f1 score	5.349E-03	6.463E-03	4.800E-03	5.819E-03
mean value	recall	0.9140	0.9112	0.9157	0.9125
	precision	0.9599	0.9472	0.9590	0.9426
	f1 score	0.9311	0.9227	0.9328	0.9213

Table 5: Results of category 3 of FASHIONMNIST with gaussian symmetrical noise

		QRCNN	CNN(leaky-relu)	QDCNN	CNN(rot-relu)
variance	recall	1.628E-02	1.320E-02	1.363E-02	1.556E-02
	precision	7.740E-03	8.798E-03	6.703E-03	9.586E-03
	f1 score	7.353E-03	6.443E-03	6.118E-03	7.401E-03
mean value	recall	0.8960	0.9023	0.9047	0.8930
	precision	0.9312	0.9254	0.9391	0.9234
	f1 score	0.9056	0.9068	0.9154	0.9003

Table 6: Accuracy on FASHIONMNIST with symmetrical noise

	QRCNN	HQNet	QDCNN
mixed noise	0.9003	0.9011	0.9280
gaussian noise	0.9157	0.9194	0.9294
uniform noise	0.9165	0.9096	0.9380

Table 7: Accuracy on MNIST with symmetrical noise

	QRCNN	HQNet	QDCNN
mixed noise	0.9472	0.9532	0.9680
gaussian noise	0.9506	0.9491	0.9794
uniform noise	0.9412	0.9405	0.9711

Table 8: Accuracy on FASHIONMNIST with unsymmetrical noise

	QRCNN	HQNet	QDCNN
mixed noise	0.8957	0.8787	0.9270
gaussian noise	0.9003	0.9096	0.9201
uniform noise	0.9241	0.9190	0.9422

Table 9: Accuracy on MNIST with unsymmetrical noise

	QRCNN	HQNet	QDCNN
mixed noise	0.9494	0.9305	0.9682
gaussian noise	0.9311	0.9435	0.9603
uniform noise	0.9487	0.9475	0.9622

precision. Their definitions are follows:

$$Accuracy = \frac{TP + TN}{TP + TN + FP + FN}. \quad (13)$$

$$Recall = \frac{TP}{TP + FN}. \quad (14)$$

$$Precision = \frac{TP}{FP + TP}. \quad (15)$$

$$f1\ score = \frac{2 \times Precision \times Recall}{Precision + Recall}, \quad (16)$$

where True Positive (TP) denotes the number of samples of a category truly predicted as positive if we regard this category as positive in a dataset and other categories in the dataset negative. True Negative (TN) is the number of samples predicted as negative that is negative. False Positive (FP) is the number of samples that are incorrectly predicted to be negative but are positive in fact. False Negative (FN) represents the number of samples that are falsely predicted to be positive but are actually negative. The P-R curve plots precision against recall at different classification thresholds, while the ROC curve plots true positive rate against false positive rate at assorted classification thresholds. They are expected to be close to 1 [2]. Furthermore, we utilize iris data with three categories and MNIST, FASHIONMNIST, CIFAR100 image datasets with each image dataset comprised of four categories. The iris data is 4-dimensional, the size of MNIST and FASHIONMNIST is $28 \times 28 \times 1$, while that of CIFAR dataset is $32 \times 32 \times 3$. In terms of each dataset, we set 75% of it as training set and 25% of it as testing set. And

the proportion of each category of data in each dataset is approximately the same. To emulate real-world scenarios more closely, the noises added are pure symmetrical and pure unsymmetrical gaussian noises, pure symmetrical and pure unsymmetrical uniform noises, and mixed noises with symmetrical and asymmetric distributions, a total of six cases [44, 45, 46]. The symmetrical noise means the noise data distribution which is symmetrical with respect to the y-axis in a Cartesian coordinate system (see supplementary material part 12) [45]. These noises used in the paper are significant in engineering control [44]. There are more types of asymmetric noise than symmetric noise [44]. Therefore, in the engineering field, the probability of asymmetric noise occurring is more than that of symmetric noise [44, 47]. Moreover, to add more uncertainties to simulate the situations of real world, the amount and the position of the noise added to the data are both random in each group of the experiment [45]. And in each group of generalization power experiment, the noisy dataset utilized for training and testing all the models is identical.

Table 1 to Table 5 demonstrate the outcomes of FASHIONMNIST with pure gaussian symmetrical noise (more results of other datasets in supplementary materials part 7). The results include the P-R and ROC curve area and accuracy. They also incorporate variances and mean values of precision, recall and f1 score of the four categories, from category 0 to category 3. And the category Y ($Y=0,1,2,3$) means a category labeled as the number Y. The mean value is the average values of precision, recall and f1 score of all the samples in a certain category from the 100th epoch to the 300th epoch after convergence, which implies the learning ability of models for samples of different categories. The variance represents that of precision, recall and f1 score of all the samples in a certain category from the 100th epoch to the 300th epoch after convergence, which indicates the degree of fluctuation of the indicators, reflecting the stability of the models. As for Table 1, while the accuracy of QRCNN and the two

CNNs is 92.84%, 92.99% and 93.10%, that of QDCNN is 93.16%, which is slightly higher than that of QRCNN and CNNs. However, the accuracy difference between these models is exceedingly small. And the differences of P-R and ROC curve area between the four models are very small as well. Table 2 shows the variances and mean values of recall, precision and f1 score of category 0 of noisy FASHIONMNIST with category 0 considered as positive and other categories regarded as negative. Table 3 shows the variances and mean values of recall, precision and f1 score of category 1 of noisy FASHIONMNIST with category 1 considered as positive and other categories regarded as negative. Table 4 shows the variances and mean values of recall, precision and f1 score of category 2 of noisy FASHIONMNIST with category 2 considered as positive. Table 5 shows the variances and mean values of recall, precision and f1 score of category 3 of noisy FASHIONMNIST with category 3 considered as positive. As for the Table 2 to Table 5, there are only very small discrepancy of the variances and mean values of the three metrics between the four models. And the outcomes in part 7 in the supplementary materials also indicate the exceedingly small discrepancy of those. Therefore, our hybrid models could not outperform pure classical models in all these indicators. They only perform approximately on par with classical CNNs on datasets with symmetrical noises on various metrics. What's more, Table 6 and 7 demonstrate accuracy of HQNet, QRCNN as well as QDCNN on noisy FASHIONMNIST and MNIST respectively. The results point the slight superiority of QDCNN over QRCNN and HQNet. While QRCNN shows approxiamtely as high accuracy as the HQNet model, more significantly, the accuracy of QDCNN is about 2%-3% higher than HQNet and QRCNN models, which shows the ascendancy of the dense connection of the convolutional and quantum-inspired layers in QDCNN.

5.1.1. Test on datasets with unsymmetrical noises

Table 8 and 9 show the accuracy of three models on noisy FASHIONMNIST and MNIST respectively. The outcomes also reveal the slightly more prominent performance of QDCNN with 2%-3% higher accuracy over HQNet and QRCNN. Other results of the comparison between our hybrid models and classical MLPs and CNNs are shown in the part 7 of the supplementary material. On the whole, the outcomes indicate that our hybrid models possess roughly the same level of generalization capability as MLPs or CNNs in recognizing data containing asymmetric noises.

5.2. Robustness test

Robustness is appraised by the same metrics in generalization power part. And in this part, we use the same datasets as in generalization power part. For QDFNN, QRFNN and the MLPs, in each group of robustness experiments, we randomly choose one layer and attack some parameters randomly in the layer utilizing the six noises in generalization power test. The layer indices and the number of parameters that are chosen for attacking in the layer of the three models are identical. In terms of QRCNN, QDCNN, CNNs and HQNet, since we hope to evaluate the robustness of the fully connected layers of these models, we randomly choose a fully-connected layers in the CNNs, a quantum-inspired layer in QRCNN and QDCNN, a quantum layer in HQNet for attacking. And we ensure the layer indices and the number of parameters attacked in the layer in CNNs is also exactly the same as that in HQNet and our QDCNN and QRCNN. In each group of robustness experiment, the noise used to attack different models is exactly the same. Nonetheless, the noise used for attacking and the number of parameters chosen in one layer for attacking between different groups of experiments are different. There are two common attacking forms: ① $\sigma(\theta + \epsilon)$ and ② $\sigma(\theta) + \epsilon$, where θ is the parameter and ϵ is the noise. σ represents activation operations in pure

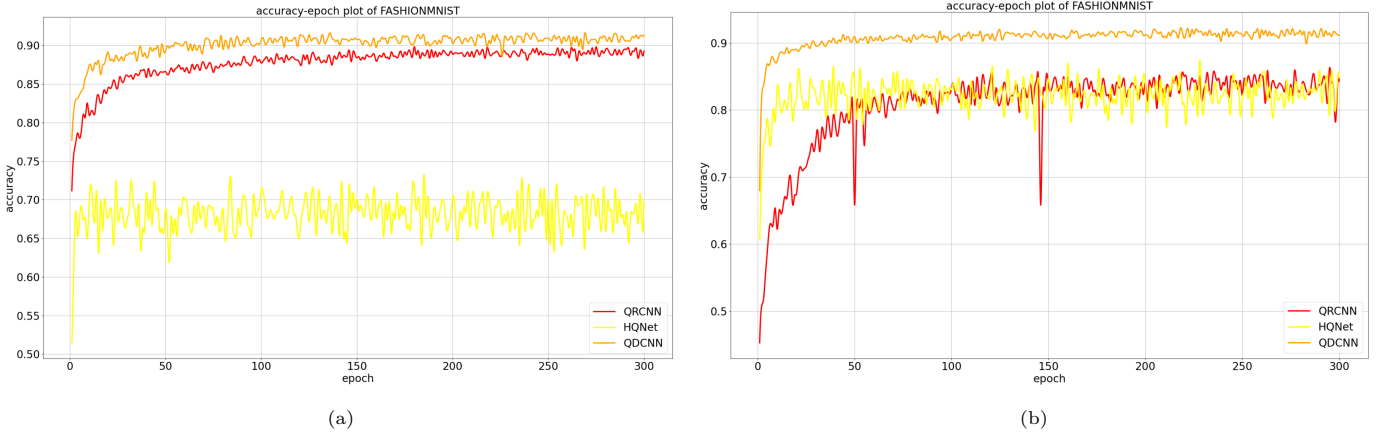


Figure 5: Accuracy results under symmetrical mixed noise attacks on FASHIONMNIST. We utilize a state-of-the-art HQNet for comparison. (a) Parameter attack in form ①. (b) Parameter attack in form ②. We can see that as for (a), the average accuracy of QDCNN is slightly higher than that of QRCNN and much higher than that of HQNet. In terms of (b), while the accuracy of HQNet and QRCNN is very close, that of QDCNN is higher than it.

Table 10: Accuracy on FASHIONMNIST under symmetrical noise attacking

noise type	form	QRCNN	HQNet	QDCNN
mixed	①	0.8879	0.6839	0.9075
mixed	②	0.8326	0.8242	0.9130
gaussian	①	0.8634	0.8792	0.9109
gaussian	②	0.8701	0.8893	0.9267
uniform	①	0.8943	0.8742	0.9214
uniform	②	0.9045	0.9001	0.9148

classical models or sine and cosine functions in our hybrid models or HQNet[44, 48, 49, 50]. The test of robustness is separated into symmetrical noise attack with form ①,② and unsymmetrical noise attack with form ①,②. The accuracy value is the average accuracy value after the models reach convergence. The link to the program codes is on the last page of this paper.

5.2.1. Test under symmetrical noise attacking

Fig.5 and Table 10 demonstrate the accuracy of HQNet, QRCNN and QDCNN on FASHIONMNIST under symmetrical attacks in the two forms. From the outcomes, QRCNN does not outperform HQNet, but QDCNN directly shows more advantages with the densely-connected architecture over QRFNN and HQNet. For instance, under mixed noise attacking in form ②, while the accuracy

Table 11: Accuracy on FASHIONMNIST under unsymmetrical noise attacking

		CNN(rot-relu)	QRCNN	CNN(leaky-relu)	QDCNN
Fig.(6a)	accuracy	23.00%	73.65%	25.00%	78.67%
	loss	nan	0.0085	nan	0.0082
Fig.(6b)	accuracy	21.00%	75.96%	25.00%	76.10%
	loss	nan	0.0063	nan	0.0079
Fig.(7a)	accuracy	27.00%	91.86%	25.00%	93.02%
	loss	nan	0.0012	nan	0.0027
Fig.(7b)	accuracy	24.00%	89.71%	25.00%	92.94%
	loss	nan	0.0014	nan	0.0018

of QRCNN and HQNet is 83.26% and 82.42%, that of QDCNN is 91.30%, which is 8%-9% higher than that of HQNet and QRCNN. Comparison results between pure classical models and our hybrid models are in the part 8 of the supplementary material. Sometimes our hybrid models show slight more prominent performance than classical models, while the results of classical models are marginally better than that of our hybrid models at times. On the whole, our hybrid models indicate roughly the same level of capability as classical models in resistance to symmetrical noise attacks.

5.2.2. Test under unsymmetrical noise attacking

More importantly, our hybrid models show much greater superiority over classical models under unsymmetrical noise attacks in the two forms (see supplementary ma-

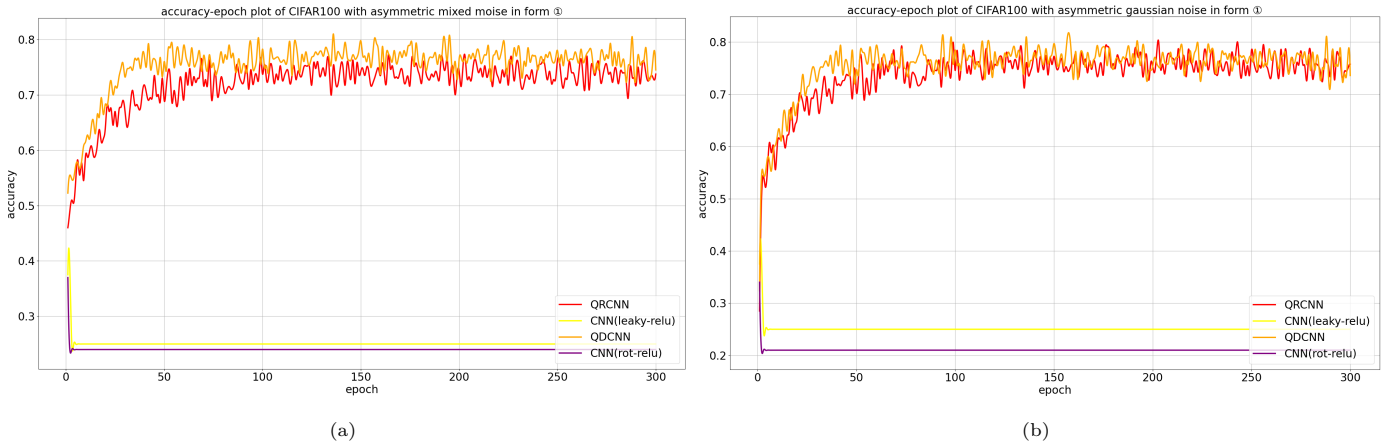


Figure 6: Unsymmetrical noise attack in form ① in CIFAR100. We utilize two pure classical CNNs for comparison, of which the activation functions are separately rot-relu and leaky-relu functions. (a) Parameter attack with mixed unsymmetrical noise. (b) Parameter attack with gaussian unsymmetrical noise. In terms of the average test accuracy of the two pure classical models, the results remain low values in (a) and (b) since the loss reach nan.

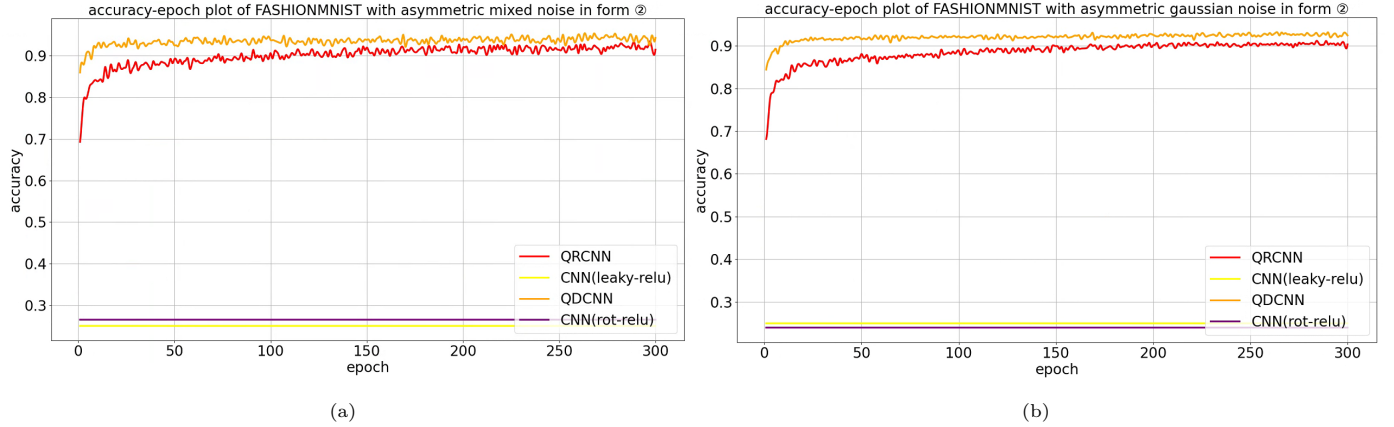


Figure 7: Accuracy under unsymmetrical noise attack in form ② on FASHIONMNIST. We utilize two pure classical CNNs for comparison, of which the activation functions are separately rot-relu and leaky-relu function. (a) Parameter attack with mixed unsymmetrical noise. (b) Parameter attack with gaussian unsymmetrical noise. In terms of the average test accuracy of the two pure classical models, the results remain low values in (a) and (b) since the loss reach nan.

Table 12: Accuracy on FASHIONMNIST under unsymmetrical noise attacking

noise type	form	QRCNN	HQNet	QDCNN
mixed	①	0.8278	0.8401	0.8999
mixed	②	0.6833	0.7380	0.9187
gaussian	①	0.7993	0.7612	0.9056
gaussian	②	0.8596	0.8478	0.9125
uniform	①	0.7934	0.8150	0.9073
uniform	②	0.8092	0.8445	0.9177

terials part 8 for more results). Fig.6 shows the accuracy under gaussian and mixed asymmetric attack in form ①

on CIFAR100. As for Fig.(6a), while the accuracy of two CNNs is only 25% and 23%, that of QDCNN and QRCNN is 78.67% and 73.65% respectively, which shows the advantages of the quantum-inspired layers of our hybrid architectures. And there are also a little more superiority of QDCNN over QRCNN. The accuracy results of the four models in Fig.(6b) is similar with that in Fig.(6a). Fig.7 demonstrates the accuracy under gaussian and mixed asymmetric attacks in form ② on FASHIONMNIST. In the two figures, the accuracy of the pure classical models

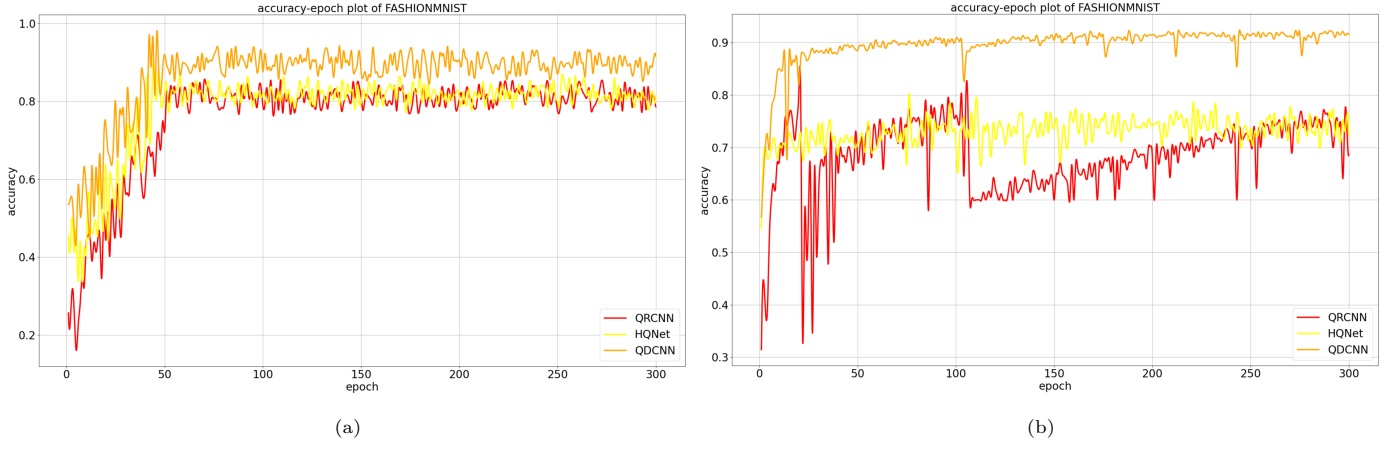


Figure 8: Accuracy under unsymmetrical mixed noise attacks on FASHIONMNIST. We utilize a state-of-the-art HQNet for comparison. (a) Parameter attack in form ①. (b) Parameter attack in form ②.

maintains at a low value around 25%, which shows that the pure classical models fail to learn the features. And we find the loss curves of the pure classical models oscillate badly and the loss values are very large and up to nan, which implies the reason of the bad performance of the pure classical models is gradient explosion (see part 9 of the supplementary material). However, even under various unsymmetrical noise attacks with the two forms, our hybrid models still show great performance on the tasks with the accuracy being 90% roughly due to the quantum-inspired layers in our hybrid models to avoid gradient explosion. And Table 11 shows the average accuracy values of the curves in Fig.6 and Fig.7.

Moreover, Fig.8 as well as Table 12 indicate the accuracy of QRCNN, QDCNN and HQNet under assorted asymmetrical noises attacks with the two forms on FASHIONMNIST. Both Fig.(8a) and (8b) shows the accuracy of the three models with that of QDCNN greater than HQNet and QRCNN, which points the advantages of the combination of dense connection with the convolutional layers and the symmetrical circuit model. In Fig.(8b), the fluctuation degree of QRCNN is slightly higher than that of QDCNN and HQNet, which shows the instability of QRCNN. However, the average accuracy of QRCNN and HQNet in Table 12 is close, which shows the same level of performance of

them.

5.2.3. Ablation study

To test the advantages of the adaptive residual and dense connection of our hybrid models, we use **T**raditional **Q**uantum-inspired **F**eedforward **N**eural **N**etwork (TQFNN) and **T**raditional **Q**uantum-inspired **C**onvolutional **N**eural **N**etwork (TQCNN) for comparison. The framework of TQFNN is exactly the same as that of QRFNN and QDFNN but without residual or dense connection. Similarly, the architecture of TQCNN is also identical to that of QRCNN and QDCNN but without residual or dense connection in the convolutional and fully connected layers as well. Hence, through theoretical analysis in the part 4 of the supplementary material, the TQFNN, QRFNN and QDFNN models are close in the computational and parameter complexity. Moreover, experimental results demonstrate that the accuracy of our hybrid models is approximately 2%-3% higher than that of TQFNN and TQCNN. For example, as for Fig.(9a), the accuracy of TQFNN on clean iris data is 87.93%, while that of QRFNN and QDFNN is 89.57% and 92.55%. It indicates the superiority of the adaptive residual and dense connections in our hybrid models over the quantum-inspired neural networks without residual or dense connection. Furthermore, QDFNN and QDCNN outperform QRFNN and QRCNN

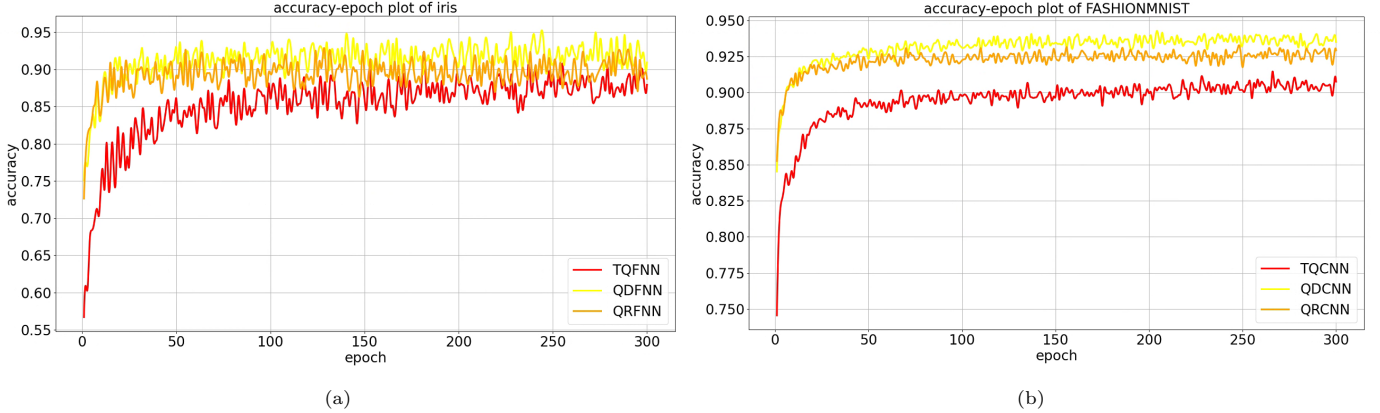


Figure 9: Test accuracy of the traditional quantum-inspired neural network and our hybrid models with noiseless datasets. (a) Accuracy results of noiseless iris data of TQFNN, QRFNN and QDFNN. (b) Accuracy results of noiseless FASHIONMNIST data of TQCNN, QRCNN and QDCNN. The average accuracy of TQCNN is 90.19%, while that of QRCNN and QDCNN is 92.52% and 93.55%. It indicates the slightly more advantage of the dense connection in QDCNN over the residual connection in QRCNN. Additionally, our two hybrid models outperform TQCNN, which shows the function of the residual and dense connections.

a little separately, which shows the more advantages of the dense connection in QDFNN and QDCNN over the residual connection in QRFNN and QRCNN.

6. Conclusion and discussion

To summarize, we have firstly proposed the hybrid quantum-inspired neural networks combining symmetrical circuit model with adaptive residual or dense connections. We explain their frameworks and assess their generalization power and robustness. HQNet and Classical MLP, CNNs with concrete structures and quantum-inspired neural networks without residual or dense connection are used for comparison. The charm of our hybrid models lies in these facts that:

- Under the premise that the computational and parameter complexity of our hybrid models and the traditional quantum-inspired network without residual or dense connection are close, our hybrid models show 2%-3% higher accuracy over the quantum-inspired neural networks;
- They show the same level of generalization ability and robustness as the MLPs and CNNs when the datasets

contain the six noises, or the parameters are attacked by symmetrical noises;

- They show much more outstanding robustness than the MLPs and CNNs with the parameters attacked by unsymmetrical noises;
- The densely-connected frameworks possess slightly more superiority over HQNet on classification tasks with noisy datasets used;
- The densely-connected frameworks are more advantageous than HQNet on classification tasks under the attacks of symmetrical and asymmetrical noises;
- They raise potential to systematically prevent the gradient explosion problem.

While the quantum-inspired layers enhance the robustness and prevent gradient explosion, the adaptive residual and dense connections facilitate feature learning and generalization power of our hybrid models. Therefore, the novelty of our models lies in the combination of adaptive residual or dense connection with the quantum-inspired layers with symmetrical circuits, which improves the comprehensive performance in the neural network field. Hence,

our hybrid models are able to substitute pure classical or other quantum-inspired neural networks in certain tasks. However, according to the part 5 of the supplementary material, the computational complexity of QRFNN, $C_{QRFNN} \approx B \cdot I \cdot L \cdot N^4 \propto N^4$, and the computational complexity of QDFNN, $C_{QDFNN} \approx B \cdot I \cdot L \cdot N^4 \propto N^4$, where B and I are batchsize and number of iterations in an epoch separately. Since $N = 2^n$, $C_{QRFNN} \propto 2^{4n}$, and $C_{QDFNN} \propto 2^{4n}$, where n is the number of qubit. It indicates the trouble to expand the dimension of the quantum state in the quantum-inspired layer, which is also the width of our hybrid neural networks [19, 51]. If our hybrid models are used for large-scale datasets, the computational complexity of them could will increase exponentially, leading to a large amount of time consumption. Therefore, our models are more suitable for problems on data of modest-scale dimension of the feature space, such as iris data in scikit-learn library [31]. Nonetheless, when it comes to the design of deep neural networks, our work may herald a future where the hybrid architectures redefine the boundaries of deep learning to unprecedented heights. What's more, owing to the outstanding generalization capability and robustness of our hybrid models, it makes sense to leverage them on complicated noisy engineering environments [47]. The links of the supplementary material and program codes are below the acknowledgements.

CRediT authorship contribution statement

Andi Chen: Conceptualization, Data curation, Formal analysis, Investigation, Methodology, Software, Validation, Visualization, Writing – original draft, Writing – review & editing. **Hua-Lei Yin:** Writing – review & editing. **Zeng-Bing Chen:** Writing – review & editing. **Shengjun Wu:** Writing – review & editing.

Acknowledgements

This work is supported by the National Natural Science Foundation of China (Grants No. 12175104 and

No. 12274223), the Innovation Program for Quantum Science and Technology (2021ZD0301701), the National Key Research and development Program of China (No. 2023YFC2205802), the Key Research and Development Program of Nanjing Jiangbei New Area (No.ZDYD20210101), the Program for Innovative Talents and Entrepreneurs in Jiangsu (No. JSSCRC2021484), and the Program of Song Shan Laboratory (Included in the management of Major Science and Technology Program of Henan Province) (No. 221100210800-02).

[Click here for supplementary material information](#)

[Click here for corresponding codes](#)

References

- [1] Y. LeCun, Y. Bengio, G. Hinton, Deep learning, *nature* 521 (2015) 436–444. doi:10.1038/nature14539.
- [2] I. Goodfellow, Y. Bengio, A. Courville, Deep learning, MIT press, 2016.
- [3] S. J. Prince, Understanding Deep Learning, MIT press, 2023.
- [4] J. Schmidhuber, Deep learning in neural networks: An overview, *Neural networks* 61 (2015) 85–117. doi:10.1016/j.neunet.2014.09.003.
- [5] N. Buduma, N. Buduma, J. Papa, Fundamentals of deep learning, O'Reilly Media, Inc., 2022.
- [6] Y. Guo, Y. Liu, A. Oerlemans, S. Lao, S. Wu, M. S. Lew, Deep learning for visual understanding: A review, *Neurocomputing* 187 (2016) 27–48. doi:10.1016/j.neucom.2015.09.116.
- [7] J. Ngiam, A. Khosla, M. Kim, J. Nam, H. Lee, A. Y. Ng, Multi-modal deep learning, in: Proceedings of the 28th international conference on machine learning (ICML-11), 2011, pp. 689–696. doi:10.5555/3104482.3104569.
- [8] K. He, X. Zhang, S. Ren, J. Sun, Deep residual learning for image recognition, in: Proceedings of the IEEE conference on computer vision and pattern recognition, 2016, pp. 770–778. doi:10.1109/CVPR.2016.90.
- [9] G. Huang, Z. Liu, L. Van Der Maaten, K. Q. Weinberger, Densely connected convolutional networks, in: Proceedings of the IEEE conference on computer vision and pattern recognition, 2017, pp. 4700–4708. doi:10.1109/CVPR.2017.243.
- [10] W. X. Zhao, K. Zhou, J. Li, T. Tang, X. Wang, Y. Hou, Y. Min, B. Zhang, J. Zhang, Z. Dong, et al., A survey of large language models, *arXiv preprint arXiv:2303.18223* (2023). doi:10.48550/arXiv.2303.18223.

[11] Y. Liu, K. Zhang, Y. Li, Z. Yan, C. Gao, R. Chen, Z. Yuan, Y. Huang, H. Sun, J. Gao, et al., Sora: A review on background, technology, limitations, and opportunities of large vision models, arXiv preprint arXiv:2402.17177 (2024). doi:10.48550/arXiv.2402.17177.

[12] I. A. Basheer, M. Hajmeer, Artificial neural networks: fundamentals, computing, design, and application, *Journal of microbiological methods* 43 (2000) 3–31. doi:10.1016/S0167-7012(00)00201-3.

[13] S. B. Laughlin, T. J. Sejnowski, Communication in neuronal networks, *Science* 301 (2003) 1870–1874. doi:10.1126/science.1089662.

[14] J. Wang, A. Pal, Q. Yang, K. Kant, K. Zhu, S. Guo, Collaborative machine learning: Schemes, robustness, and privacy, *IEEE Transactions on Neural Networks and Learning Systems* (2022). doi:10.1109/TNNLS.2022.3169347.

[15] K. Zhou, Z. Liu, Y. Qiao, T. Xiang, C. C. Loy, Domain generalization: A survey, *IEEE Transactions on Pattern Analysis and Machine Intelligence* (2022). doi:10.1109/TPAMI.2022.3195549.

[16] P. R. Bassi, S. S. Dertkigil, A. Cavalli, Improving deep neural network generalization and robustness to background bias via layer-wise relevance propagation optimization, *Nature Communications* 15 (2024) 291. doi:10.1038/s41467-023-44371-z.

[17] P. J. Coles, Seeking quantum advantage for neural networks, *Nature Computational Science* 1 (2021) 389–390. doi:10.1038/s43588-021-00088-x.

[18] W. Ye, R. Liu, Y. Li, L. Jiao, Quantum-inspired evolutionary algorithm for convolutional neural networks architecture search, in: 2020 IEEE Congress on Evolutionary Computation (CEC), IEEE, 2020, pp. 1–8. doi:10.1109/CEC48606.2020.9185727.

[19] S. Song, Y. Hou, G. Liu, The interpretability of quantum-inspired neural network, in: 2021 4th International Conference on Artificial Intelligence and Big Data (ICAIBD), IEEE, 2021, pp. 294–298. doi:10.1109/ICAIBD51990.2021.9459009.

[20] L.-J. Wang, J.-Y. Lin, S. Wu, Implementation of quantum stochastic walks for function approximation, two-dimensional data classification, and sequence classification, *Physical Review Research* 4 (2022) 023058. doi:10.1103/PhysRevResearch.4.023058.

[21] D. Szwarcman, D. Civitarese, M. Vellasco, Quantum-inspired neural architecture search, in: 2019 International Joint Conference on Neural Networks (IJCNN), IEEE, 2019, pp. 1–8. doi:10.1109/IJCNN.2019.8852453.

[22] K. Mitarai, M. Negoro, M. Kitagawa, K. Fujii, Quantum circuit learning, *Physical Review A* 98 (2018) 032309. doi:10.1103/PhysRevA.98.032309.

[23] Y. Liang, W. Peng, Z.-J. Zheng, O. Silvén, G. Zhao, A hybrid quantum–classical neural network with deep residual learning, *Neural Networks* 143 (2021) 133–147. doi:10.1016/j.neunet.2021.05.028.

[24] N. Schetakis, D. Aghamalyan, P. Griffin, M. Boguslavsky, Review of some existing qml frameworks and novel hybrid classical–quantum neural networks realising binary classification for the noisy datasets, *Scientific Reports* 12 (2022) 11927. doi:10.1038/s41598-022-14876-6.

[25] D. Konar, A. D. Sarma, S. Bhandary, S. Bhattacharyya, A. Cangi, V. Aggarwal, A shallow hybrid classical–quantum spiking feedforward neural network for noise-robust image classification, *Applied Soft Computing* 136 (2023) 110099. doi:10.1016/j.asoc.2023.110099.

[26] P. Li, H. Xiao, F. Shang, X. Tong, X. Li, M. Cao, A hybrid quantum-inspired neural networks with sequence inputs, *Neurocomputing* 117 (2013) 81–90. doi:10.1016/j.neucom.2013.01.029.

[27] A. Wang, D. Mao, X. Li, T. Li, L. Li, Hqnet: A hybrid quantum network for multi-class mri brain classification via quantum computing, *Expert Systems with Applications* 261 (2025) 125537. URL: <https://www.sciencedirect.com/science/article/pii/S0957417424024047>. doi:<https://doi.org/10.1016/j.eswa.2024.125537>.

[28] Y.-Y. Hong, C. L. P. P. Rioflorido, W. Zhang, Hybrid deep learning and quantum-inspired neural network for day-ahead spatiotemporal wind speed forecasting, *Expert Systems with Applications* 241 (2024) 122645. URL: <https://www.sciencedirect.com/science/article/pii/S0957417423031470>. doi:<https://doi.org/10.1016/j.eswa.2023.122645>.

[29] A. Sagingalieva, M. Kordzanganeh, A. Kurkin, A. Melnikov, D. Kuhmistrov, M. Perelshtein, A. Melnikov, A. Skolik, D. V. Dollen, Hybrid quantum resnet for car classification and its hyperparameter optimization, *Quantum Machine Intelligence* 5 (2023). doi:10.1007/s42484-023-00123-2.

[30] W. R. Clements, P. C. Humphreys, B. J. Metcalf, W. S. Kolthammer, I. A. Walmsley, Optimal design for universal multiport interferometers, *Optica* 3 (2016) 1460–1465. doi:10.1364/OPTICA.3.001460.

[31] F. Pedregosa, G. Varoquaux, A. Gramfort, V. Michel, B. Thirion, O. Grisel, M. Blondel, P. Prettenhofer, R. Weiss, V. Dubourg, et al., Scikit-learn: Machine learning in python, *the Journal of machine Learning research* 12 (2011) 2825–2830. URL: <http://jmlr.org/papers/v12/pedregosa11a.html>.

[32] A. Krizhevsky, I. Sutskever, G. E. Hinton, Imagenet classification with deep convolutional neural networks, in: F. Pereira, C. Burges, L. Bottou, K. Weinberger (Eds.), *Advances in Neural Information Processing Systems*, volume 25, Curran Associates, Inc., 2012, pp. 84–90. doi:10.1145/3065386.

[33] S. Ren, K. He, R. Girshick, J. Sun, Faster r-cnn: Towards real-time object detection with region proposal networks, *IEEE transactions on pattern analysis and machine intelligence* 39 (2016) 1137–1149. doi:10.1109/TPAMI.2016.2577031.

[34] Q. Chen, Y. Wang, T. Yang, X. Zhang, J. Cheng, J. Sun, You only look one-level feature, in: *Proceedings of the IEEE/CVF conference on computer vision and pattern recognition*, 2021, pp. 13039–13048. doi:10.1109/CVPR46437.2021.01284.

[35] Y. Lin, I. Koprinska, M. Rana, Ssdnet: State space decomposition neural network for time series forecasting, in: *2021 IEEE International Conference on Data Mining (ICDM)*, IEEE, 2021, pp. 370–378. doi:10.1109/ICDM51629.2021.00048.

[36] H. Zhao, J. Shi, X. Qi, X. Wang, J. Jia, Pyramid scene parsing network, in: *Proceedings of the IEEE conference on computer vision and pattern recognition*, 2017, pp. 2881–2890. doi:10.1109/CVPR.2017.660.

[37] J. Deng, W. Dong, R. Socher, L.-J. Li, K. Li, L. Fei-Fei, Imagenet: A large-scale hierarchical image database, in: *2009 IEEE conference on computer vision and pattern recognition*, Ieee, 2009, pp. 248–255. doi:10.1109/CVPR.2009.5206848.

[38] S. Minaee, Y. Boykov, F. Porikli, A. Plaza, N. Kehtarnavaz, D. Terzopoulos, Image segmentation using deep learning: A survey, *IEEE transactions on pattern analysis and machine intelligence* 44 (2021) 3523–3542. doi:10.1109/TPAMI.2021.3059968.

[39] A. Hering, L. Hansen, T. C. Mok, A. C. Chung, H. Siebert, S. Häger, A. Lange, S. Kuckertz, S. Heldmann, W. Shao, et al., Learn2reg: comprehensive multi-task medical image registration challenge, dataset and evaluation in the era of deep learning, *IEEE Transactions on Medical Imaging* 42 (2022) 697–712. doi:10.1109/TMI.2022.3213983.

[40] Z. Li, F. Liu, W. Yang, S. Peng, J. Zhou, A survey of convolutional neural networks: analysis, applications, and prospects, *IEEE transactions on neural networks and learning systems* 33 (2021) 6999–7019. doi:10.1109/TNNLS.2021.3084827.

[41] A. Vaswani, N. Shazeer, N. Parmar, J. Uszkoreit, L. Jones, A. N. Gomez, L. Kaiser, I. Polosukhin, Attention is all you need, *Advances in neural information processing systems* 30 (2017) 6000–6010. doi:10.5555/3295222.3295349.

[42] G. Chiribella, G. M. D’Ariano, P. Perinotti, Quantum circuit architecture, *Physical review letters* 101 (2008) 060401. doi:10.1103/PhysRevLett.101.060401.

[43] F. Milletari, N. Navab, S.-A. Ahmadi, V-net: Fully convolutional neural networks for volumetric medical image segmentation, in: *2016 fourth international conference on 3D vision (3DV)*, Ieee, 2016, pp. 565–571. doi:10.1109/3DV.2016.79.

[44] C. H. H. Bies, David A., C. Q. Howard, *Engineering Noise Control*, CRC Press, 2017. doi:10.1201/9781351228152.

[45] M. D. Schmidt, H. Lipson, Learning noise, in: *Proceedings of the 9th annual conference on Genetic and evolutionary computation*, 2007, pp. 1680–1685. doi:10.1145/1276958.1277289.

[46] B. Kosko, K. Audhkhasi, O. Osoba, Noise can speed backpropagation learning and deep bidirectional pretraining, *Neural Networks* 129 (2020) 359–384. doi:10.1016/j.neunet.2020.04.004.

[47] N. Semenova, L. Larger, D. Brunner, Understanding and mitigating noise in trained deep neural networks, *Neural Networks* 146 (2022) 151–160. doi:10.1016/j.neunet.2021.11.008.

[48] Y. Xiao, M. Adeogok, C.-S. Leung, K. W. Leung, Robust noise-aware algorithm for randomized neural network and its convergence properties, *Neural Networks* (2024) 106202. doi:10.1016/j.neunet.2024.106202.

[49] Y. Shen, J. Wang, Robustness analysis of global exponential stability of recurrent neural networks in the presence of time delays and random disturbances, *IEEE transactions on neural networks and learning systems* 23 (2011) 87–96. doi:10.1109/TNNLS.2011.2178326.

[50] D. F. Nettleton, A. Orriols-Puig, A. Fornells, A study of the effect of different types of noise on the precision of supervised learning techniques, *Artificial intelligence review* 33 (2010) 275–306. doi:10.1007/s10462-010-9156-z.

[51] Z. Lu, H. Pu, F. Wang, Z. Hu, L. Wang, The expressive power of neural networks: A view from the width, *Advances in neural information processing systems* 30 (2017). doi:10.5555/3295222.3295371.